

Solid State Stability Studies of Model Dipeptides: Aspartame and Aspartylphenylalanine

SUZANNE S. LEUNG[‡] AND DAVID J. W. GRANT[×]

Received May 23, 1996, from the *Department of Pharmaceutics, College of Pharmacy, University of Minnesota, Weaver-Densford Hall, 308 Harvard St. S.E., Minneapolis, MN 55455-0343*. Final revised manuscript received July 23, 1996. Accepted for publication July 25, 1996[⊗]. [‡]Present address: 3M Pharmaceuticals, 270-4S-17, 3M Center, St. Paul, MN 55144.

Abstract □ Some solid-state pharmaceutical properties and the solid-state thermal stability of the model dipeptides aspartame (APM) and aspartylphenylalanine (AP), have been investigated. Studies by differential scanning calorimetry (DSC), thermal gravimetric analysis (TGA), high-performance liquid chromatography, powder X-ray diffraction, and optical microscopy have shown that the dipeptides undergo solid state intramolecular aminolysis of the type, solid → solid + gas. This reaction was observed for APM at 167–180 °C with the liberation of methanol and for AP at 186–202 °C with the liberation of water. The exclusive solid product of the degradation reaction of both dipeptides is the cyclic compound 3-(carboxymethyl)-6-benzyl-2,5-dioxopiperazine. The rates of the degradation reactions were monitored by isothermal TGA and by temperature-ramp DSC and were found to follow kinetics based on nucleation control with activation energies of about 266 kJ mol⁻¹ for APM and 234 kJ mol⁻¹ for AP.[‡]

Introduction

While the solution reactions of small peptides have been quite well-characterized (e.g., Scheme 1),¹ their reactions in the solid state have attracted scant attention. With the increasing use of small peptides as pharmaceuticals, it is important to understand the solid-state behavior of this important class of compound. In the present study, aspartame (APM) and aspartylphenylalanine (AP) are used as models for small peptides. These dipeptides are suitable candidates for solid-state studies because of their relatively low cost. APM (L-aspartyl-L-phenylalanine methyl ester), a dipeptide sweetener, is finding increasing use in foods, beverages, and pharmaceuticals. The present report describes the physical properties of solid APM and solid AP and evaluates their chemical stabilities.

Solid-state reactions may be classified as physical transformations or chemical reactions.² Physical transformations include polymorphic transitions and desolvations and are characterized by changes in the crystal structure without modifications of the component molecules. Chemical reactions of the solid state include rearrangements, photochemical reactions, and decompositions. Physical transformations of aspartame will be discussed in a later publication.

Thorough solid-state stability studies of aspartame have not been previously reported. Lack of solid-state stability results in loss of the active ingredient. In addition, the presence of the reaction product as an impurity may alter the properties of the solid. The major labile bonds in aspartame are the amide and the ester bonds. In aqueous solution, aspartame degradation occurs via multiple pathways, as shown in Scheme 1.¹ Without the methoxy group, the bond that is most sensitive to hydrolysis in AP is the amide bond. The present evaluation of the stability of APM and AP in the solid state may contribute to a general understanding of the solid-state

chemistry of small peptides. A preliminary report of this work has been recently presented.³

Materials and Methods

Materials—APM, AP, and 3-(carboxymethyl)-6-benzyl-2,5-dioxopiperazine (DKP) were gifts from the NutraSweet Company, Mount Prospect, IL. Sodium heptanesulfonate was obtained from Eastman Kodak Chemical Co., Rochester, NY. Sodium phosphate monobasic, phosphoric acid, and 1,1,1-trichloroethane (all ACS grade) were obtained from Fisher Scientific, Fairlawn, NJ, as were water and acetonitrile (both HPLC grade). All materials were used without further modification or purification.

Differential Scanning Calorimetry (DSC)—The DSC curves were determined using a DuPont 910 differential scanning calorimeter (TA Instruments, New Castle, DE) equipped with a data station (Thermal Analyst 2000, TA Instruments, New Castle, DE). The cell constant was calibrated using indium. Samples (2.50–2.70 mg) in nonhermetically crimped or open aluminum pans were heated at 0.5, 1, 2, 4, 7, and 10 °C/min under nitrogen purge at 3–4 mL/min. The peak temperature was noted as the point on the temperature scale corresponding to maximum deviation from the baseline.

Thermogravimetric Analysis (TGA)—The TGA curves were obtained using a DuPont 951 thermogravimetric analyzer (TA Instruments, New Castle, DE) linked to a data station (Thermal Analyst 2000, TA Instruments, New Castle, DE). All TGA runs were performed on samples in open aluminum pans with a nitrogen purge at 3–4 mL/min. Nonisothermal TGA was performed on samples (2.30–2.50 mg) at a heating rate of 10 °C/min. Isothermal TGA was performed on APM samples (2.20–2.50 mg) at 166.9, 170.4, 175.5, and 180.3 °C and for AP samples (2.20–2.50 mg) at 186.2, 191.9, 196.5, and 202.0 °C.

Karl Fischer Titrimetry—The water content of APM and AP samples was determined by Karl Fischer titrimetry using a Mitsubishi Moisture Meter (Model CA-05, Mitsubishi Chemical Industries Ltd., Tokyo, Japan).

Particle Size Analysis—Powder samples of APM and AP were suspended in 1,1,1-trichloroethane by sonication and analyzed in a particle size analyzer (Brinkmann 2010, Westbury, NY) with mechanical stirring.

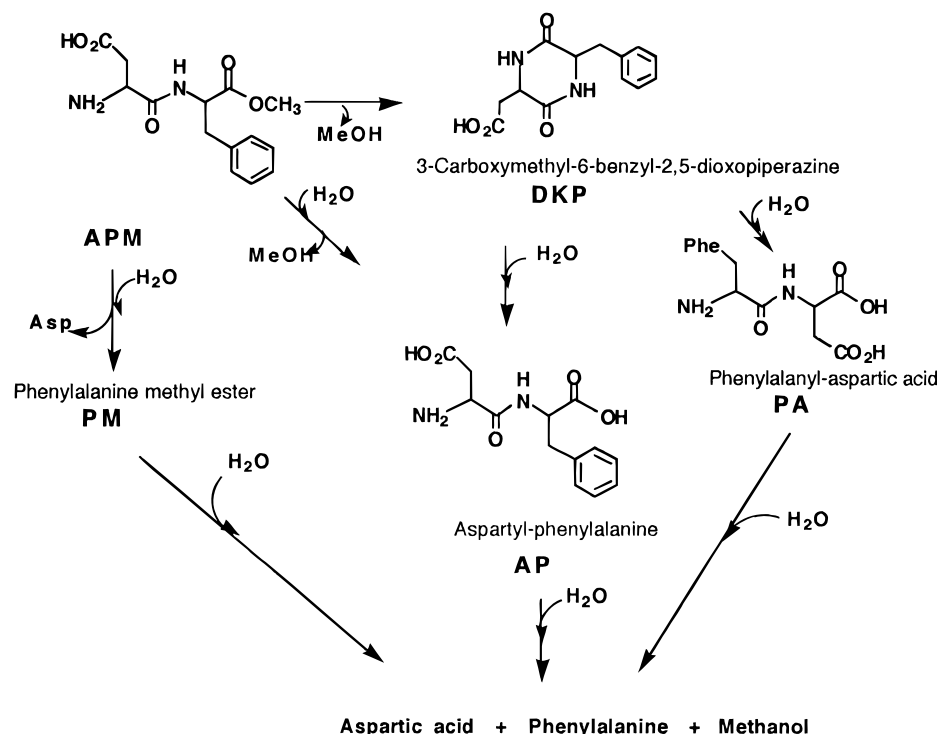
Surface Area Measurements—The specific surface area of powder samples of APM and AP particles was determined using multipoint nitrogen adsorption by the dynamic volumetric BET method (Gemini 2360, Micromeritics, Norcross, GA).

Density—The density of the samples was determined by a helium-air pycnometer (Autopycnometer 1320, Micromeritics, Norcross, GA).

Powder X-ray Diffractometry (PXRD)—The powder X-ray diffraction patterns of APM and AP samples were determined at ambient temperature using an X-ray powder diffractometer (Siemens D-500, Germany) at 30 mA and 45 kV with Cu K α radiation. Counts were measured using a scintillation counter. Samples were packed into an aluminum holder and scanned with the diffraction angle, 2θ , increasing from 5° to 35°, with a step size of 0.02° and a counting time of 1 s.

High-Performance Liquid Chromatography (HPLC)—HPLC was used to separate and identify APM, AP, and their degradation products according to the method of Stamp and Labuza.⁴ For the present study, the HPLC system (Shimadzu Scientific, Chicago, IL) consisted of a liquid chromatograph (LC-6A), an autoinjector (SIL-6A), a system controller (SCL-6A), a UV detector (SPD-6AV), and a printer (Chromatopac CR-5A). The column (Nova-pak C18) and guard column (Guardpak C18) were obtained from Waters Associates,

[⊗] Abstract published in *Advance ACS Abstracts*, September 1, 1996.



Scheme 1—Pathways of APM degradation in aqueous solution. The ionic charges, which depend on pH, are not shown.

Milford, MA. The mobile phase consisted of 4 mM sodium heptane-sulfonate and 4 mM sodium phosphate monobasic in 20% acetonitrile in water, adjusted to pH 3.0 with phosphoric acid. The flow rate was 1.0 mL/min and the detection wavelength was 214 nm.

Hot Stage Microscopy—Optical micrographs were obtained with a hot stage (Mettler FP 80, Mettler Instrument Corporation, Hightstown, NJ) mounted on an optical microscope (Wild M3Z, Wild Heerbrugg, Heerbrugg, Switzerland) equipped with photoautomat (Wild MPS45) and a 35 mm camera attachment. Crystals were immersed in high boiling silicone oil (Aldrich Chemical Co., Milwaukee, WI) and heated at a rate of 3 °C/min.

Molecular Modeling—The program Cerius² (Molecular Simulations, Burlington, MA) was run on Silicon Graphics Indigo hardware to predict the low-energy conformers of APM. Conformers were searched via a grid scan with a step size of 30°, varying the torsional angles, ψ , ϕ , and χ , of APM. Because of the size of the calculation, the torsional angles of the aspartyl and the phenylalanyl residues were varied separately. Each conformer was minimized and the lowest energy conformer was used to vary the remaining torsional angles. All energy calculations employed the universal force field⁵ while charges were calculated using the charge equilibration method,⁶ both available on Cerius².

Results and Discussion

Stability of Aspartame—The physical properties of APM, as received, are listed in Table 1. The total amount of water in APM samples, determined by Karl Fischer titrimetry, was higher than that for the phase-pure hemihydrate (2.97% water), suggesting that the samples contained sorbed water. The particle size number distribution followed a log-normal relationship with a number-length mean diameter of 8.3 ± 1.1 μm.

DSC of APM in crimped pans gave three endotherms (Figure 1a). TGA with the same temperature program (10 °C/min) gave two weight loss steps (Figure 1b), which correspond to the first two DSC endotherms. The first DSC endotherm at 129 °C and the first TGA weight loss step at about 114 °C are attributed to loss of water, i.e. dehydration of the crystal lattice, as indicated by Karl Fischer titration.

Table 1—Physical Properties of Aspartame (APM) and Aspartylphenylalanine (AP) as Received

| | APM ^a | AP ^a |
|---|--------------------------|--------------------------|
| Appearance | White crystalline powder | White crystalline powder |
| Habit | Acicular | Acicular |
| Density (g/cm ³) | 1.49 ± 0.04 | 1.17 ± 0.04 |
| Specific surface area (m ² /g) | 2.29 ± 0.07 | 3.41 ± 0.10 |
| Particle size (μm) ^b | 8.3 ± 0.6 | 7.9 ± 0.5 |
| Water Content (% w/w) ^c | 3.76 ± 0.05 | 0.162 ± 0.045 |
| After heating to 150 °C | 0.33 ± 0.05 | |

^a Mean ± SD (n = 3). ^b Particle size followed a log-normal relationship with the number-length mean diameter stated. ^c Water content determined by Karl Fischer titrimetry.

The water content of APM samples heated to 140 °C and cooled to ambient was 0.33 ± 0.05%. The second DSC endotherm at 189 °C and the second TGA weight loss step at about 196 °C require more detailed study, presented and discussed below. The third DSC endotherm at 248 °C was not accompanied by a TGA weight loss step and corresponds to the reported melting point of 248 °C.⁷

A sample of APM crystals was placed in silicone oil and heated at 3 °C/min under a hot stage microscope. Vapor was released as bubbles from the needle-shaped crystals at approximately 110 °C, consistent with desolvation at the first endotherm. However, the crystals also released a vapor at approximately 190 °C (Figure 2b), corresponding to the second weight loss step in TGA at 196 °C and to the second DSC endotherm at 189 °C. The crystals did not disintegrate or change shape even under vigorous gas evolution. However, the crystals darkened after the second stage of gas evolution at 190 °C (Figure 2). Formation of liquid was not observed until 248 °C, the reported melting point of APM.⁷

Since APM readily degrades in aqueous solution, its degradation in the solid state was investigated as the possible origin of the endotherm, weight loss, and release of vapor at about 190 °C. In solution, the major degradation products of

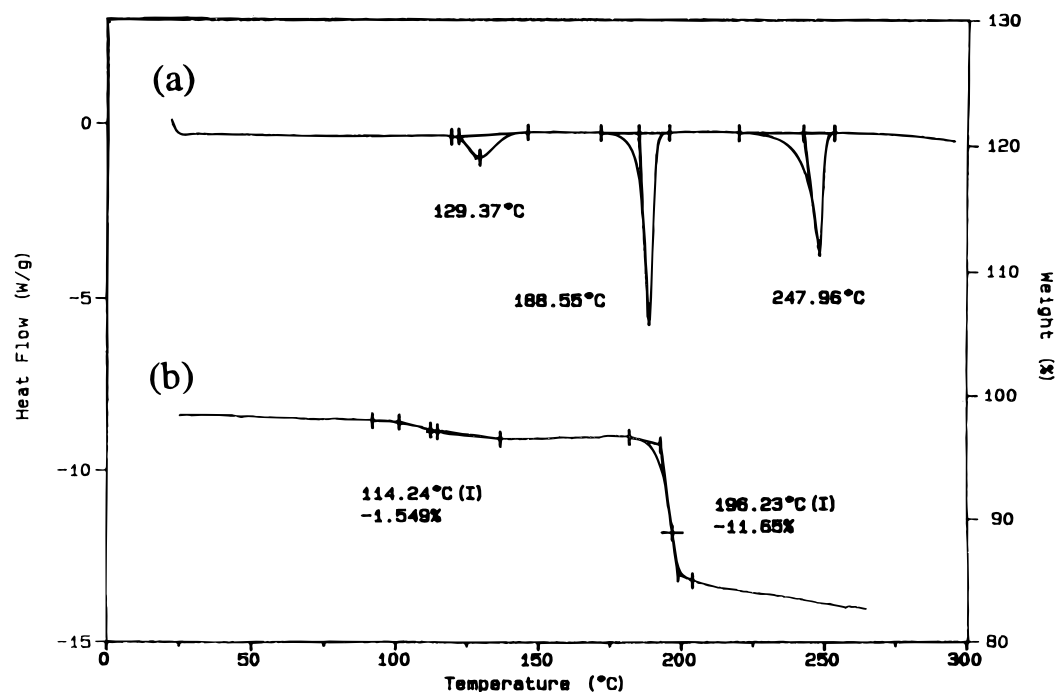


Figure 1—DSC and TGA curves for APM: (a) DSC curve corresponding to the left axis and (b) weight loss by TGA corresponding to the right axis. The change from 23 to 150 °C corresponds to the dehydration of APM, which is the subject of a subsequent report.⁸

APM are AP and DKP. AP is formed by direct hydrolysis of the ester linkage, while DKP is formed by intramolecular aminolysis. In the solid state either reaction would result in the release of methanol with a theoretical weight loss of 10.55%, close to the observed weight loss of $11.13 \pm 0.59\%$ in TGA (Figure 1b). This close comparison suggests that heating APM in the solid state results in degradation with the liberation of methanol.

The possible formation of AP and/or DKP on heating solid APM was investigated by HPLC and PXRD. For this purpose, the HPLC chromatogram in Figure 3a shows the separation of the pure compounds, APM (the starting material), and AP and DKP (the presumed degradation products), while parts a and b of Figure 4 show the quite distinct PXRD patterns of APM and DKP, respectively. The effects of heating APM to the different temperatures were compared. A 2.6 mg sample of APM was heated in the DSC to 150 °C, beyond the first DSC endotherm and TGA step, which are attributed to dehydration, but was removed before the second endotherm and TGA step (Figure 1) and then cooled and analyzed by HPLC. The product gave an HPLC chromatogram (Figure 3b) the peak of which corresponded to pure unchanged APM (retention time of 7.16 min). The PXRD pattern of APM at 150 °C corresponded to that of anhydrous APM and was different from that of the starting material.⁸

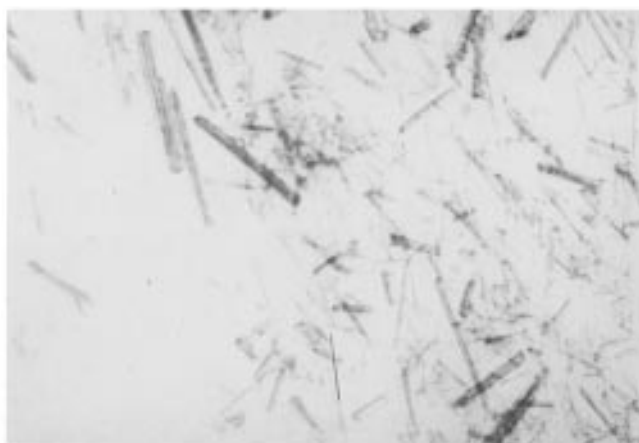
Another 2.6 mg sample was heated in the DSC to 200 °C, beyond the second DSC endotherm and TGA step but before the third endotherm (Figure 1), and was similarly analyzed. The product gave an HPLC chromatogram (Figure 3c) with a single peak corresponding to pure DKP, with no detectable traces of other degradation products nor of the starting material, APM. The PXRD pattern of the product (Figure 4c) showed that it was crystallographically identical to DKP (Figure 4b) and that diffraction peaks due to APM were absent. However, Figure 4c shows broad background scattering (amorphous halo) centered around $20^\circ 2\theta$, suggesting that the DKP formed by the solid-state degradation of APM was less crystalline than the DKP standard. This lower crystallinity is manifested in a DSC melting point of 248 °C

(Figure 1a), below 259 ± 1.1 °C for the pure crystalline standard DKP. DKP decomposes on melting.

To summarize the results from DSC and TGA (Figure 1), the first DSC endotherm and TGA step are attributed to dehydration of the APM crystals. The hydration and dehydration behaviors of APM are the subject of another report. The second DSC endotherm and TGA step are attributed to the solid-state decomposition of APM with gas evolution due to loss of methanol according to Scheme 3. The third DSC endotherm at 248 °C (Figure 1), which has been attributed to melting of APM,⁷ actually corresponds to the melting of DKP that results from the degradation of solid APM.

Intramolecular cyclization is the major pathway of degradation of APM in solution. However, cyclization was not expected to be the major pathway of degradation in the solid state because the large conformational change necessary to bring the nucleophilic amine in proximity to the ester carbonyl would presumably require room which, at first sight, would appear to be lacking in the solid state due to the packing of the molecule in the crystal lattice.

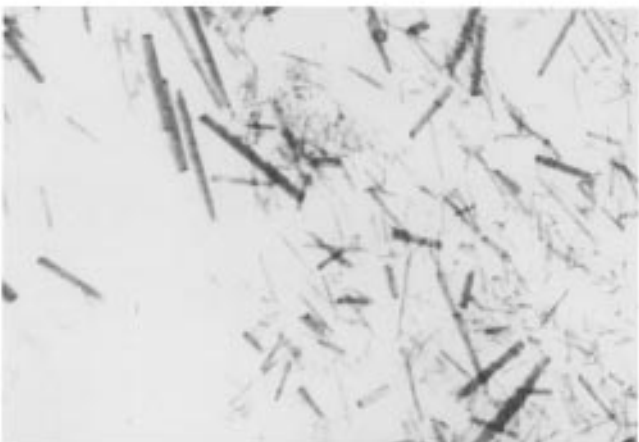
The path of a nucleophile attacking a carbonyl carbon is described by the Bürgi–Dunitz trajectory.⁹ By reference to crystal structures of compounds containing nucleophilic and electrophilic groups, the reaction coordinate for nucleophilic addition was mapped. The N, C, and the O atoms lie in a mirror plane, while the C atom deviates from the plane defined by R, R', and O (Scheme 2).¹⁰ The extent of deviation increases as the C...N distance, *d*, decreases. As the nitrogen atom approaches the carbon atom, the C–O bond lengthens and the alkyl substituents bend away. The nitrogen atom approaches at an angle, α , of 107° with little variation between the different crystal structures. The value of α is similar for other nucleophilic additions. The N...C–R angle ranges from 82 to 120° . If this reaction coordinate can be applied to APM, the molecule must undergo considerable rearrangement in order to bring the nucleophilic nitrogen along this path. Although a crystal structure of APM hemihydrate has been determined,¹¹ it does not correspond to the commercially available polymorph⁸ and one can only speculate on the



(a)



(b)



(c)

Figure 2—Optical micrographs of APM crystals at various temperatures: (a) at 150 °C, (b) at 190 °C, and (c) at 200 °C.

structure of the commercially available form. However, most dipeptides exist in their extended conformations in the solid state with the side chains arranged in an antiparallel fashion,¹² and the commercially available polymorph of APM may be no exception.

The flexibility of the APM molecule may explain the occurrence of intramolecular cyclization. A search for low-energy conformers of APM was performed by varying the torsional angles φ and χ of the aspartyl residue and the torsional angles ψ , ϕ , and χ of the phenylalanyl residue at

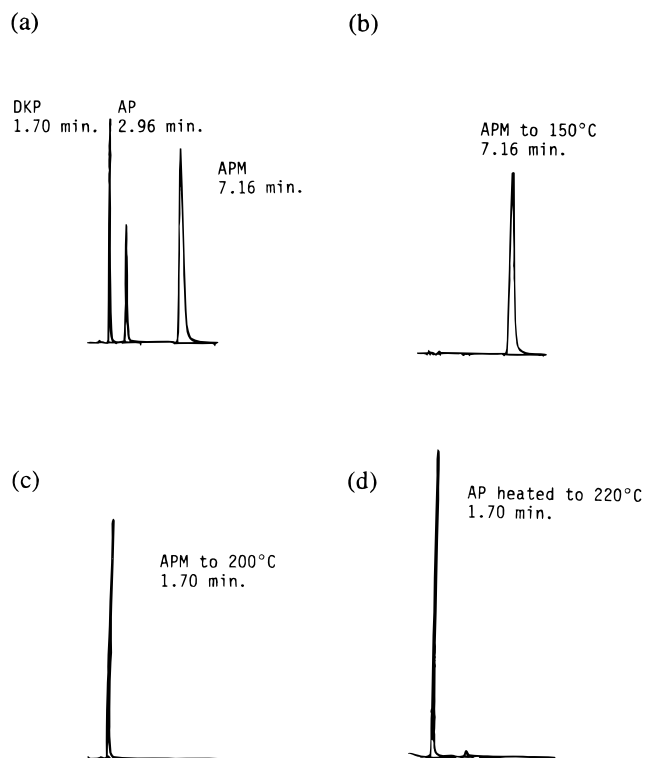


Figure 3—HPLC chromatograms of (a) prepared mixtures of the pure compounds APM, AP and DKP, (b) the product obtained by heating APM to 150 °C, (c) the product obtained by heating APM to 200 °C, and (d) the product obtained by heating AP to 220 °C.

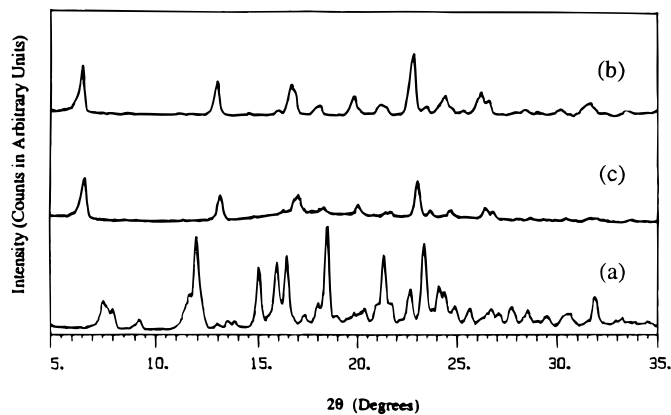
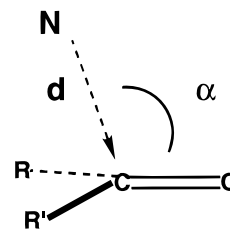
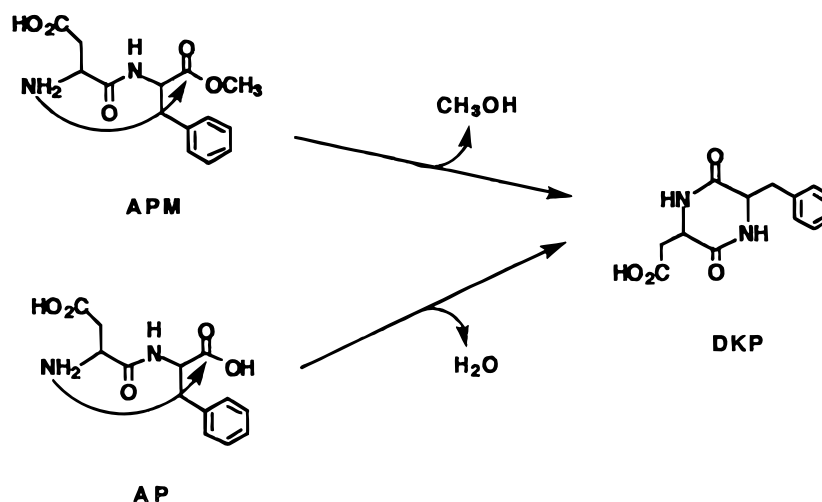


Figure 4—Powder X-ray diffraction patterns of (a) APM, (b) DKP, and (c) the solid product obtained by heating APM to 200 °C.



Scheme 2—The trajectory of a nucleophilic nitrogen in an addition reaction.

30° increments using the grid scan method. The resulting conformers were minimized and the five lowest energy conformers were calculated and are overlaid in Figure 5. The low-energy conformers exist in similar conformations in the aspartyl residue. Side chain conformation is governed by the electrostatic interaction between the positively charged protonated amino group and the negatively charged γ -carboxy-



Scheme 3—Solid state intramolecular aminolysis reactions of APM and AP leading to solid DKP.

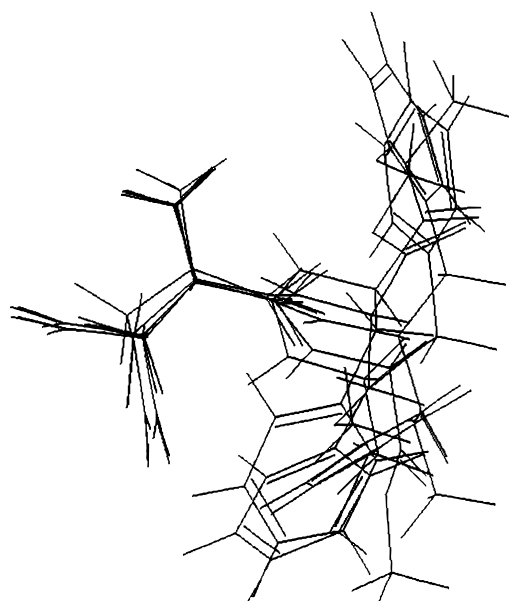


Figure 5—The five lowest energy conformers of APM are overlaid.

late. The phenylalanyl residue showed significant variation in conformation among the different conformers. This result is similar to that for hydrated APM reported by Kang,¹³ who selected low-energy conformations of APM analogs as starting points for minimization, while no such assumption was made here. Variations in the conformation of the phenylalanyl residue was also found in the crystal structure of $[(APM)_2-Cu] \cdot \frac{8}{3}H_2O$.^{8,14} The large differences between the low-energy conformers suggest that APM is very flexible. The geometry of the five lowest energy conformers is not far from the Bürgi–Dunitz trajectory.¹⁰ The $N \cdots C=O$ angles range from 110.5° to 125.8° and the $N \cdots C-OMe$ angles range from 85.2° to 109.9° , close to 107° and 82° – 120° respectively, the values obtained by Bürgi.¹⁰ Although the conformation of APM in the solid state may differ from the low-energy conformations found in the conformer search, at the elevated temperature of the reaction, thermal disruption of the lattice may allow the APM molecules to change their conformation. Conformational changes to a lower energy state may actually bring the attacking nucleophile along the reaction coordinate for cyclization.

The alternative pathways to DKP formation, hydrolysis of the amide bond to give phenylalanine methyl ester and direct

hydrolysis of the ester bond to give aspartylphenylalanine, would presumably require less rearrangement within the crystal lattice. DKP formation appears to contradict the topochemical postulate that reactions in the solid state proceed with a minimum of molecular motion. The correlation of reactant and product geometries in many solid-state reactions is the basis of this theory. The similar geometries of the reactant and product arise from the confinement of the molecular rearrangements to a cavity defined by the crystal lattice. Examples of non-topochemical reactions include photochemical polymerizations of vinyl monomers.¹⁵ Although large molecular motions in the lattice are hindered at room temperature, at the elevated temperatures at which intramolecular aminolysis occurs, molecules in the solid may acquire sufficient energy to overcome the steric barriers to rearrangement.

In aqueous solution the abundance of water allows the hydrolysis of APM, to form AP and PM, to compete with DKP formation. However, in the solid-state, at the temperature of the solid state reaction (about $190^\circ C$), desolvation of the lattice water has already occurred and adsorbed water would likewise have evaporated. Although intramolecular cyclization would seem unlikely, it might happen because other pathways that require water for hydrolysis are not available.

Stability of Aspartylphenylalanine—To look into the possible uniqueness or otherwise of intramolecular aminolysis as a mechanism of degradation, the solid-state stability of AP was evaluated. While AP is a product of the degradation of APM in solution, it is also a dipeptide that may be capable of undergoing intramolecular cyclization. Some physical properties of AP were determined and are listed in Table 1. As with APM, the particle size number distribution of AP follows a log-normal relationship.

The DSC profile of AP in Figure 6a shows two endotherms, the first at $211^\circ C$ and the second at $240^\circ C$. These thermal events were not baseline-separated. The corresponding TGA plot in Figure 6b shows weight loss at $217^\circ C$, corresponding closely to the first endotherm. Under hot stage microscopy, the solid to liquid transition began at $225^\circ C$. The barely measurable amount of water in the AP samples, determined by Karl Fischer titrimetry, and the lack of a dehydration endotherm at lower temperatures indicate the absence of lattice water in AP.

The two DSC endotherms observed with AP are in the same range as the second and third endotherms of APM, as if an analogous reaction were occurring with AP. In the case of AP, intramolecular attack to give DKP would release water instead of methanol. The weight loss observed by TGA, 6.44

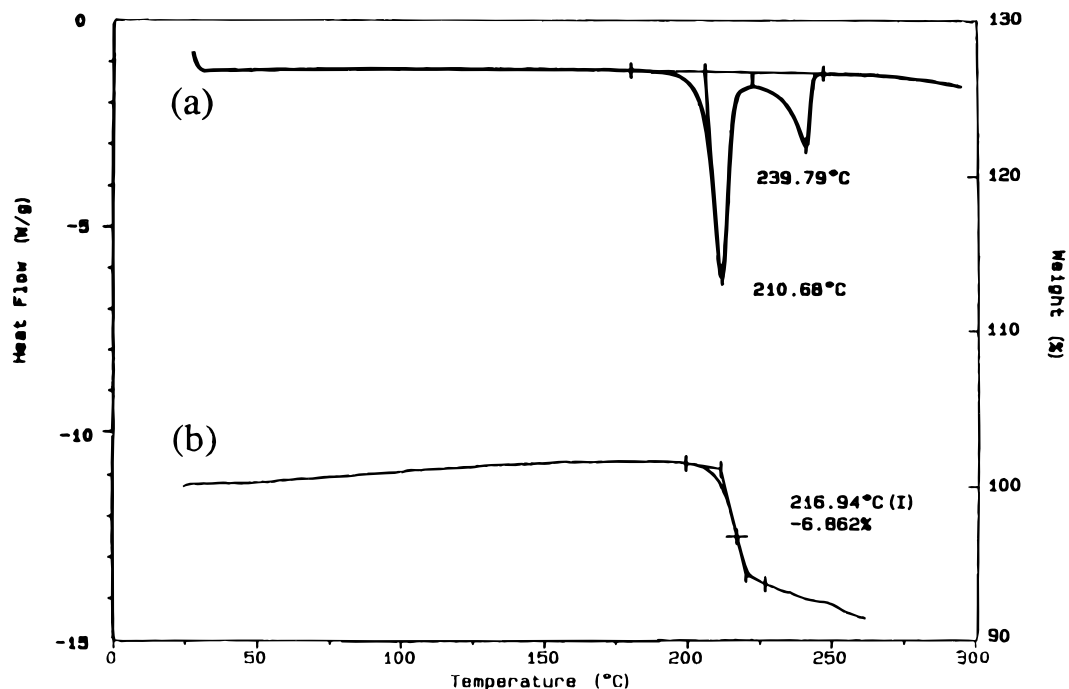


Figure 6—DSC and TGA curves for AP: (a) DSC curve corresponding to the left axis and (b) weight loss by TGA corresponding to the right axis.

$\pm 0.33\%$ (Figure 6b), compares favorably with the theoretical weight loss of 6.42% for liberation of 1 mol equiv of water from AP. Under hot stage optical microscopy, the evolution of vapor was seen at 210–220 °C.

The formation of DKP was confirmed by HPLC analysis of heated AP samples (Figure 3). At 220 °C, a temperature beyond the first and before the second endotherm, the sample of AP showed complete conversion to DKP, proving that the endotherm at 211 °C is caused by the intramolecular cyclization of AP to form DKP, with release of water. The temperature at which this reaction occurs for AP (about 211 °C) is higher than for APM (about 190 °C). As DKP is formed, it begins to melt, corresponding to the second endotherm. Scheme 3 shows the reaction for both APM and AP. For AP, the alternative reaction to DKP formation is hydrolysis of the amide bond. As in the case of APM, this hydrolysis reaction is unlikely to occur due to the lack of water at this elevated temperature.

Kinetics of Cyclization of Aspartame and Aspartyl-phenylalanine—The reaction was studied by isothermal TGA at various temperatures. The fraction reacted, x , is plotted against time for APM in Figure 7. The shape of the curves is sigmoidal, as is common for solid-state decompositions.¹⁶ The curves are characterized by an induction period at low x values, a growth period with an inflection at intermediate values of x , and a decay period at high x values.

The reaction curves can be modeled by rate equations which assume various mechanisms. For APM degradation, the Prout–Tompkins equation¹⁷ was found to provide the best fit to the kinetic profile. The kinetic data for the cyclization of APM at $0.10 \leq x \leq 0.90$ were fitted with a correlation coefficient, $R = 0.9946$. The Avrami–Erofeev equation¹⁸ provides a fit ($R = 0.9930$) that is almost as close. The values of $x < 0.10$ and $x > 0.90$ are subject to variability due to the slow rate of conversion at the induction and decay periods. The residuals are randomly distributed and no trends were seen for either model. For AP degradation, the Prout–Tompkins and Avrami–Erofeev equations provide similar fits, with $R = 0.9994$ for both models; the residuals were randomly

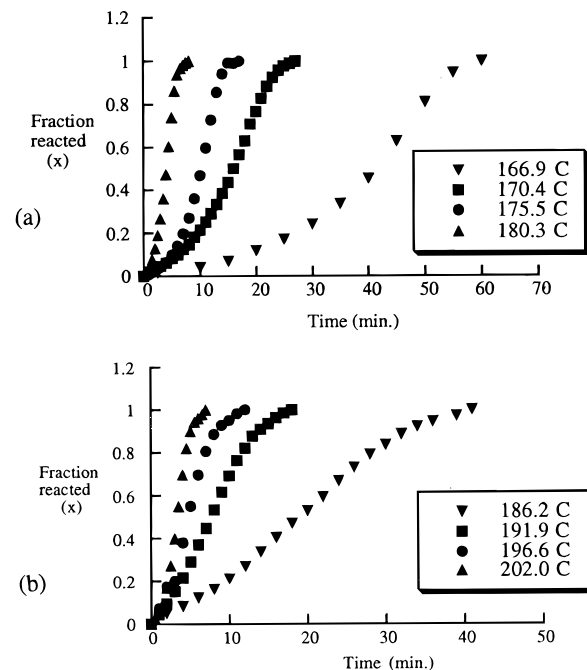


Figure 7—Plots of fraction reacted against time for the intramolecular aminolysis of (a) APM and (b) AP.

distributed and no trends were seen for either model, as for APM degradation. The activation energies, evaluated by graphical solution of the Arrhenius equation using the rate constant calculated from the Prout–Tompkins equation (Figure 8), were $268 \pm 8 \text{ kJ mol}^{-1}$ for APM and $242 \pm 8 \text{ kJ mol}^{-1}$ for AP.

The activation energies were calculated independently using temperature-ramp DSC via the Kissinger equation (eq 1),¹⁹ which relates the heating rate, ϕ (in degrees Celsius/minute), temperature at peak maximum, T_m (in degrees Kelvin), and activation energy, E_a . The activation energies for cyclization were obtained from the slope of a plot of $\ln(\phi)$

Table 2—Summary of the Thermodynamic and Kinetic Parameters for the Intramolecular Aminolysis of APM and AP and the Thermodynamic Data for Fusion of the Solid Product, DKP

| | APM ^a | AP ^a | DKP ^{a,b} |
|--|--------------------|--------------------|--------------------|
| Reaction temperature (°C) ^c | 188.9 ± 0.4 | 209.5 ± 0.8 | |
| Heat of reaction (J/g) ^d | 134.1 ± 3.1 | 198.5 ± 5.3 | |
| Melting point of solid product (°C) | 248.0 ± 1.1 | 239.4 ± 1.4 | 259.1 ± 1.1 |
| Heat of fusion of solid product (J/g) | 121.4 ± 6.1 | 78.1 ± 2.6 | 193.0 ± 15.5 |
| E _a by DSC (kJ mol ⁻¹) ^e | 265 ± 6 | 227 ± 8 | |
| E _a by TGA (kJ mol ⁻¹) ^f | 268 ± 8 | 242 ± 8 | |
| Kinetic mechanism of best fit | Nucleation control | Nucleation control | |

^a Mean value ± SD, *n* = 3. ^b The pure crystalline standard of the same chemical composition as the aminolysis product. ^c The temperature of maximum deflection of the aminolysis endotherm in DSC at the scan rate of 10 °C/min. ^d Determined from the area of the aminolysis endotherm. ^e Activation energy from slope of Figure 9, mean ± SD. ^f Activation energy from slope of Figure 8, mean ± SD.

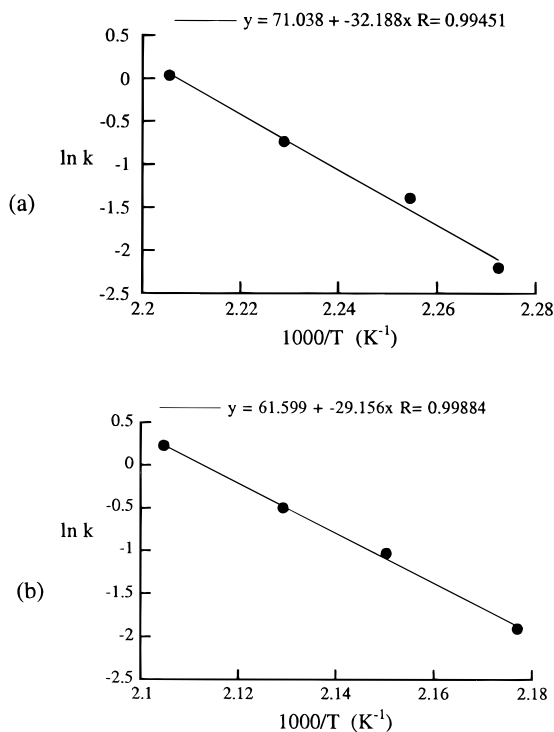


Figure 8—Arrhenius plot of the rate constants obtained for the intramolecular aminolysis of (a) APM, $E_a = 268 \pm 8 \text{ kJ mol}^{-1}$, and (b) AP, $E_a = 242 \pm 8 \text{ kJ mol}^{-1}$.

T_m^2) versus $1/T_m$ (Figure 9) and were $265 \pm 6 \text{ kJ mol}^{-1}$ for APM and $227 \pm 6 \text{ kJ mol}^{-1}$ for AP.

$$\frac{d(\ln \phi/T_m^2)}{d(1/T_m)} = -\frac{E_a}{R} \quad (1)$$

By this method, the calculated E_a values agree well with those determined by isothermal TGA. The activation energy for DKP formation from APM in the solid state is comparable with that for other solid-state chemical reactions.²⁰ The activation energy for the solid-state reaction is much greater than that for the solution reaction (70.0 kJ mol^{-1})¹ reflecting the greater energy requirement for rearrangement in the confines of a crystal lattice. The high activation energy confirms that the reaction is a true solid-state reaction of the type, solid → solid + gas.

Both the Prout–Tompkins equation and the Avrami–Erofeev equation assume that the reaction is controlled by the growth and propagation of high-energy sites or *nuclei*.^{21,22}

Nucleation can occur at these high-energy sites, such as crystal defects and surfaces. The activation energy needed for reaction at these sites of disorder is lower than in regions

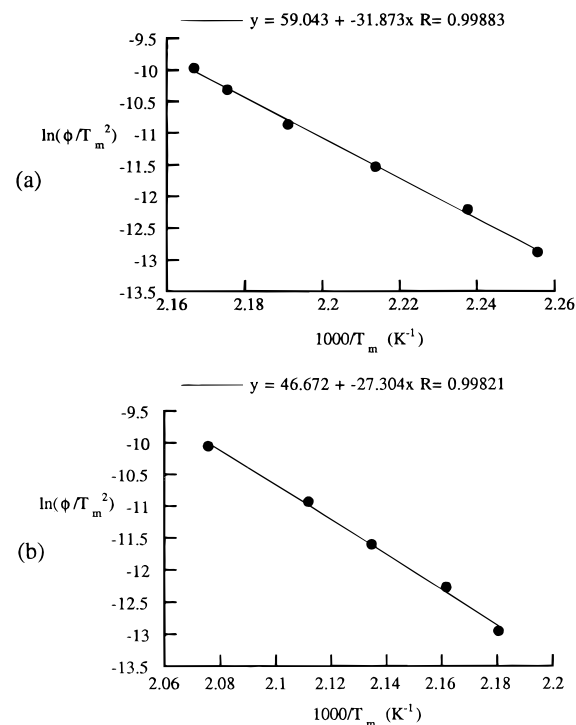


Figure 9—Kissinger plot²⁰ analyzing the effect of heating rate (ϕ , K/min) in linear temperature-ramp DSC on the peak maximum temperature, T_m of the intramolecular aminolysis of (a) APM, $E_a = 265 \pm 6 \text{ kJ mol}^{-1}$, and (b) AP, $E_a = 227 \pm 8 \text{ kJ mol}^{-1}$.

of perfect crystal packing. Once the product is formed, it becomes a source of strain in the crystal lattice and then acts as a new nucleus, disrupting the molecular interactions of the neighboring molecules and causing them to react. This chain reaction is propagated from one molecule to the next until it is terminated when and where another product molecule is encountered. This mechanism is common among non-to-chemically controlled reactions.¹⁵

Table 2 summarizes the parameters of both degradation reactions studied. AP decomposes at a slightly higher temperature than APM and with a higher enthalpy of reaction. The melting point and enthalpy of fusion of the resulting DKP are significantly lower than those of the pure crystalline material. The activation energy determined by the two methods, isothermal TGA and temperature-ramp DSC, agree well for each compound. The kinetic equations that best fit both systems were those derived assuming nucleation control, although the fact that the kinetic data follow a certain rate equation does not prove that the associated mechanism is operating.

Conclusions

Some physical properties of the model dipeptides APM and AP have been evaluated and their solid-state thermal stability determined. These dipeptides undergo solid-state intramolecular aminolysis at about 190 °C for APM, with the elimination of methanol, and at about 210 °C for AP, with the elimination of water, to form the cyclic compound 3-carboxymethyl-6-benzyl-2,5-dioxopiperazine as the exclusive solid product. For APM, the low-energy conformers appear to possess the correct geometry for cyclization. The degradation reactions for these two dipeptides were found to follow kinetics based on nucleation control with activation energies of about 266 kJ mol⁻¹ for APM and about 234 kJ mol⁻¹ for AP.

Acknowledgments

We thank the American Foundation for Pharmaceutical Education and the Pharmaceutical Research and Manufacturers of America Foundation, Inc., for consecutive predoctoral fellowships for S.S.L., the Micromeritics Instrument Corporation, Norcross, GA, for generous gifts of the Gemini 2360 surface area analyzer and the VapPrep 061, and the NutraSweet Company, Mount Prospect, IL, for gifts of APM, AP, and DKP.

References and Notes

1. Stamp, J. Kinetics and Analysis of APM Decomposition Mechanisms in Aqueous Solutions Using Multiresponse Methods. Ph.D. thesis, University of Minnesota, Minneapolis MN, 1990.
2. a. Byrn, S. Solid state organic chemistry and drug stability. *Annu. Rep. Med. Chem.* **1985**, *20*, 287–294. b. Byrn, S. *Solid State Chemistry of Drugs*; Academic Press: New York, NY, 1982; pp 59–74, 149–186.
3. Leung, S. S.; Grant, D. J. W. Solid state degradation of a model dipeptide: aspartame. *Pharm. Res.* **1995**, *12*, S-230 (PDD 7150).
4. Stamp, J.; Labuza, T. An ion-pair high performance liquid chromatographic method for the determination of APM and its decomposition products. *J. Food Sci.* **1989**, *54* (4), 1043–1046.
5. Rappé, A.; Casewit, C.; Colwell, K.; Goddard, W.; Skiff, W. UFF, a full periodic table force field for molecular mechanics and molecular dynamics simulations. *J. Am. Chem. Soc.* **1992**, *114*, 10024–10035.
6. Rappé, A.; Goddard, W. Charge equilibration for molecular dynamics simulations. *J. Phys. Chem.* **1991**, *95*, 3358–3363.
7. Budavari, S.; O'Neil, M.; Smith, A.; Heckelman, P. Eds. *The Merck Index*, Eleventh Edition, Merck & Co., Rahway, NJ, 1989, p 132.
8. Leung, S. S. Stability Studies of a Model Dipeptide, Aspartame. Ph.D. thesis, University of Minnesota, Minneapolis MN, 1996.
9. Burgi, H.; Dunitz, J. From crystal statics to chemical dynamics. *Acc. Chem. Res.* **1983**, *16*, 153–161.
10. Burgi, H.; Dunitz, J.; Shefter, E. Geometrical reaction coordinates. II. Nucleophilic addition to a carbonyl group. *J. Am. Chem. Soc.* **1973**, *95*, 5065–5067.
11. Hatada, M.; Jancarik, J.; Graves, B.; Kim, S.-H. Crystal structure of APM, a peptide sweetener. *J. Am. Chem. Soc.* **1985**, *107*, 4279–4282.
12. Görbitz, C.; Etter, M. Hydrogen bond connectivity patterns and hydrophobic interactions in crystal structures of small, acyclic peptides. *Int. J. Pept. Protein Res.* **1992**, *39*, 93–110.
13. Kang, Y. Conformation and hydration of APM. *Int. J. Pept. Protein Res.* **1991**, *38*, 79–83.
14. Ojala, W. H.; Leung, S. S.; Grant, D. J. W.; Gleason, W. B. Crystal structure of bis(aspartylphenylalanine methyl ester) copper (II). In preparation.
15. Wright, J. *Molecular crystals*, 2nd ed.; Cambridge University Press: Cambridge, UK, 1995; pp 50–70, 120–141.
16. Monkhouse, D.; Van Campen, L. Solid state reactions - theoretical and experimental aspects. *Drug Devel. Ind. Pharm.* **1984**, *10*, 1175–1276.
17. Prout, E.; Tompkins, F. The thermal decomposition of potassium permanganate. *Trans. Faraday Soc.* **1944**, *40*, 488–498.
18. Avrami, M. Granulation, phase change, and microstructure; kinetics of phase change. III. *J. Chem. Phys.* **1941**, *9*, 177–184.
19. Carstensen, J. *Drug Stability*; Marcel Dekker: New York, NY, 1990; p 132.
20. Kissinger, H. Reaction kinetics in differential thermal analysis. *Anal. Chem.* **1957**, *29*, 1702–1706.
21. Mullin, J. *Crystallization*, 3rd ed.; Butterworth-Heinemann: Oxford, UK, 1993; pp 24–27, 104–105.
22. Garner, W. Kinetics of endothermic solid reactions. In *Chemistry of the Solid State*; Garner, W., Ed.; Academic Press: New York, NY, 1955; pp 232–253.

JS960228D